The Meteoritical Society

Meteoritics & Planetary Science 49, Nr 10, 1875–1887 (2014)
doi: 10.1111/maps.12365

Mineral and chemical composition of the Jezersko meteorite—A new chondrite from Slovenia

Miloš MILER[1*], Bojan AMBROŽIČ[2], Breda MIRTIČ[2], Mateja GOSAR[1], Sašo ŠTURM[3], Matej DOLENEC[2], and Miha JERŠEK[4]

[1]Geological Survey of Slovenia, Dimičeva ulica 14, SI-1000 Ljubljana, Slovenia
[2]Faculty of Natural Sciences and Engineering, Aškerčeva 12, SI-1000 Ljubljana, Slovenia
[3]Jožef Stefan Institute, Jamova 39, SI-1000 Ljubljana, Slovenia
[4]Slovenian Museum of Natural History, Prešernova 20, SI-1001 Ljubljana, Slovenia
[*]Corresponding author: E-mail: milos.miler@geo-zs.si

(Received 21 February 2014; revision accepted 01 August 2014)

Abstract–The Jezersko meteorite is a newly confirmed stony meteorite found in 1992 in the Karavanke mountains, Slovenia. The meteorite is moderately weathered (W2), indicating short terrestrial residence time. Chondrules in partially recrystallized matrix are clearly discernible but often fragmented and have mean diameter of 0.73 mm. The meteorite consists of homogeneous olivine ($Fa_{19.4}$) and low-Ca pyroxenes ($Fs_{16.7}Wo_{1.2}$), of which 34% are monoclinic, and minor plagioclase ($Ab_{83}An_{11}Or_6$) and Ca-pyroxene ($Fs_6Wo_{45.8}$). Troilite, kamacite, zoned taenite, tetrataenite, chromite, and metallic copper comprise about 16.5 vol% of the meteorite. Phosphates are represented by merrillite and minor chlorapatite. Undulatory extinction in some olivine grains and other shock indicators suggests weak shock metamorphism between stages S2 and S3. The bulk chemical composition generally corresponds to the mean H chondrite composition. Low siderophile element contents indicate the oxidized character of the Jezersko parent body. The temperatures recorded by two-pyroxene, olivine-chromite, and olivine-orthopyroxene geothermometers are 854 °C, 737–787 °C, and 750 °C, respectively. Mg concentration profiles across orthopyroxenes and clinopyroxenes indicate relatively fast cooling at temperatures above 700 °C. A low cooling rate of 10 °C Myr^{-1} was obtained from metallographic data. Considering physical, chemical, and mineralogical properties, meteorite Jezersko was classified as an H4 S2(3) ordinary chondrite.

INTRODUCTION

An unusual brown stone was found on 13 September 1992 by a mountain hiker Mr. Božidar Jernej Malovrh while looking for a suitable resting place about 50 m southwest from a mountain hut Češka koča (1543 m.a.s.l.) at a location with coordinates 46°22′10.02″N, 14°32′7.02″E in the Karavanke mountains, Slovenia. The stony mass was lying on the surface of a grassy patch surrounded by talus gravel. Because the stone differed in color and weight from surrounding rocks and attracted a magnet, Mr. Malovrh decided to keep it and stored it in the basement at home. After more than 20 yr, Mr. Malovrh rediscovered the forgotten rock and showed it to his colleague Mr. Davorin Preisinger, who suggested taking it to the Slovenian Museum of National History (SMNH), which organized all necessary analyses. Meteorite Jezersko is the fourth meteorite and the second stony meteorite found in the territory of Slovenia.

SAMPLES AND ANALYTICAL METHODS

About 73.5 g of material was used for preparation of 6 thin sections and a polished section, ground with carborundum and polished using 6 and 3 μm diamond suspension fluids. Samples were studied under optical and electron microscopy coupled with energy dispersive X-ray spectroscopy (SEM/EDS). Optical microscopy

was carried out using a Zeiss Axio Z1 polarizing microscope in reflected and transmitted light at the Faculty of Natural Sciences and Engineering (University of Ljubljana, Slovenia). Composition of silicates was determined in thin sections using a JEOL JSM 5800 scanning electron microscope equipped with an Oxford Instruments ISIS 300 energy dispersive system at the Department for Nanostructured Materials (Jožef Stefan Institute, Slovenia). The carbon-coated thin sections were analyzed at 20 kV (Greshake et al. 1998; Sokol and Bischoff 2005) with an acquisition time of 100 s. In each silicate mineral, three EDS spectra were obtained. EDS was calibrated with a cobalt standard and the spectra were quantified using reference minerals α-quartz, albite, orthoclase, almandine, and diopside. Nonsilicate minerals were analyzed in polished section using a JEOL JSM 6490LV scanning electron microscope coupled with an Oxford Instruments INCA Energy 350 energy dispersive system at the Geological Survey of Slovenia. A carbon-coated polished section was analyzed using semiquantitative EDS analysis at 20 kV and 60 s acquisition time, optimized for quantification with a cobalt standard and the standard ZAF-correction procedure included in the INCA Energy software (Oxford Instruments 2006). Quantitative X-ray powder diffraction (XRD) was performed at the Faculty of Natural Sciences and Engineering using a Philips PW 3710 X-ray diffractometer with a Cu tube operated at 40 kV and 30 mA to obtain modal mineral composition of orthopyroxenes and high- and low-Ca clinopyroxenes. The samples were scanned from 2° to 140° θ at the speed of 0.48° 2θ min^{-1}. The data were processed using X'Pert HighScore Plus 2.2d software and ICDD-PDF-4-Minerals 2012 RDB database. Peak locations and intensities were corrected using NIST-676a standard and mineral and amorphous phases were quantitatively determined using Rietveld refinement. A piece of approximately 27 g, taken from the central part of the meteorite, was prepared for chemical analyses, performed at ActLabs, Ancaster, Canada. A 1 g aliquot was analyzed in duplicate using trace element fusion ICP-MS for contents of Cr, Cu, Zn, Ga, Ge, Rb, Mo, Cs, La, Ce, Pr, Nd, Eu, Gd, Dy, Er, and Yb. Contents of Na, Mg, Al, Si, P, K, Ca, Ti, V, Mn, Ni, Sr, and Ba in 1 g aliquot were analyzed in duplicate by fusion ICP-OES; S in 0.25 g aliquot by total digestion ICP-OES; Ru, Rh, Pd, Os, Pt, Re, and Au in 4 g aliquot by nickel sulfide fire assay INAA; and elements Sc, Fe, Co, As, Se, Br, Sb, Sm, and Ir were measured in 1.03 g aliquot by the standard INAA procedure (Activation Laboratories 2013). Accuracies of fusion ICP-MS, fusion ICP-OES, total digestion ICP-OES, nickel sulfide INAA, and standard INAA, expressed as relative errors between the measured and certified values of standard reference materials, were 4%, 5%, 8%, 3%, and 7%, respectively. Precision of trace element fusion ICP-MS and fusion ICP-OES, calculated from the relative differences between the duplicate measurements as relative percent difference, was 2%. The total analytical errors calculated for these two techniques were 8% and 7%, respectively. The overall accuracy of the results was considered to be satisfactory for all analyzed elements.

RESULTS AND DISCUSSION

Field Observations and Physical Characteristics

The site of the find is surrounded by steep mountains and extensive scree slopes consisting of Upper Triassic carbonate rocks (Mioč 1983). As no changes in surface morphology or any other indication of the impact event could be observed at the site of the find, it could be assumed that the meteorite rolled down the slope together with other scree material.

The meteorite is elongated, roughly prism-shaped single piece with square cross section (Fig. 1a). It has dimensions of 13 × 8 × 7 cm, a total mass of 1380 g prior to cutting, and density of 3.3 g cm^{-3}. One side of the meteorite is rounded and has a smooth surface, while the opposite side is rougher and contains 0.2 cm deep pits with a diameter between 0.5 and 2.2 cm (regmaglypts). The edges of the meteorite are generally well rounded. The meteorite contains several smaller and two large cracks, which probably formed during the fall or at the impact. The surface of the meteorite is mostly dark brown, in some places also light brown to reddish, due to weathering. The fusion crust is mostly well preserved; however, some smaller parts with an area of up to 2 cm^2 were chipped off. The average thickness of the fusion crust, including the layer with metal-filled veins, is 0.27 mm, while the average thickness of the outer dendritic precipitate layer is 0.04 mm. In the cross section, the meteorite shows homogeneous distribution of metallic and nonmetallic phases.

Petrography

The meteorite Jezersko has partly recrystallized porphyritic texture (Fig. 1b) varying throughout the meteorite. About 68 vol% of the meteorite is occupied by moderately sorted and well-defined chondrules and chondrule fragments. On the other hand, smaller chondrules are poorly distinguishable from the surrounding matrix. The apparent diameters of 192 measured chondrules range from 0.11 mm to 2.51 mm, with an average of 0.73 mm. The mean chondrule diameter in Jezersko is much larger than the mean diameter in H chondrites (Scott and Krot 2003;

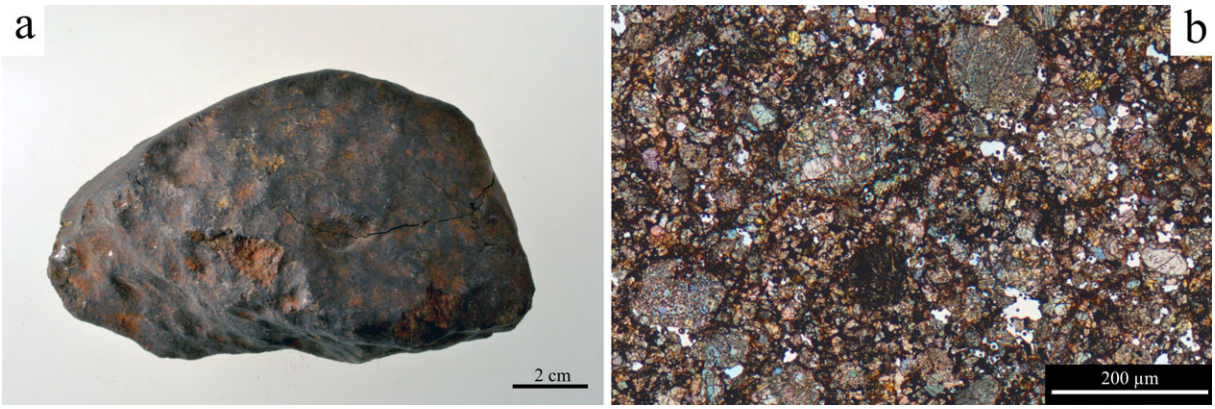

Fig. 1. Images of meteorite Jezersko. a) The meteorite had a total mass of 1380 g prior to cutting. b) Photomicrograph (transmitted light, crossed polarizers) of the Jezersko meteorite thin section showing partly recrystallized texture with relatively well-defined chondrules and chondrule fragments.

Weisberg et al. 2006), indicating that the meteorite parent body was composed of larger and inhomogeneously distributed chondrules. Chondrules are mostly oval to spherical in shape. The average eccentricity (ε) of chondrules in meteorite Jezersko is 0.58, based on the equation $\varepsilon = \sqrt{(1-(b/a)^2)}$, where b and a are mean lengths of chondrule minor and major axes, respectively. About 80% of chondrules in meteorite Jezersko are porphyritic, represented mostly by porphyritic olivine-pyroxene and porphyritic olivine chondrules, while porphyritic pyroxene chondrules occur rarely. Two different varieties of porphyritic chondrules are present. The first variety, which represents around 80% of all porphyritic chondrules, is composed of poorly sorted idiomorphic olivine grains with sizes varying from 10 μm to 500 μm and xenomorphic pyroxene grains (Fig. 2a). The chondrule matrix is composed of plagioclase and lath-shaped skeletal olivine crystals, formed probably due to reheating and melting of already existing large olivine grains, followed by quenching at cooling rate of about 80 °C h^{-1} (Donaldson 1976). The second variety is composed of tightly packed euhedral grains of olivine and pyroxene with straight grain boundaries, uniform grain size of 100 μm, and is almost completely without matrix (Fig. 2b). Textures of this variety indicate chondrules were not exposed to melting. Nonporphyritic chondrules represent 20% of chondrules in Jezersko with barred olivine textural type (Fig. 2c) constituting around 6%. Many barred olivine chondrules are of polysomatic subtype. Radial pyroxene chondrules (Fig. 2d) represent only about 5% of chondrules in Jezersko. Metal chondrules and enveloping chondrules are also present in Jezersko meteorite. Metal chondrules are composed of single grains of metal or troilite surrounded by coarse-grained olivine rim (Fig. 2e). Enveloping compound chondrules are usually made of barred olivine chondrules enveloped in large porphyritic olivine-pyroxene chondrules. Both chondrules show similar structure, implying that they merged very early in the formation history of the meteorite (Sears 2004). Some chromite-rich barred and porphyritic olivine-pyroxene chondrules with small, radially arranged acicular euhedral chromite crystals in plagioclase mesostasis as well as in pyroxene and olivine crystals were also observed (Fig. 2f). These chromite-rich chondrules are presumably secondary products indicating a very high-energy shock event (Rubin 2003). Meteorite matrix, which represents 15 vol%, is mostly brecciated and cut by shock veins filled with oxidized metal. It is mainly composed of opaque glass and microcrystalline silicate minerals, such as olivine, pyroxene, and plagioclase (Fig. 1b) with grain sizes varying between 10 μm and 100 μm. Troilite, Fe-Ni metal, chromite, and phosphates comprise about 8 vol%, 7 vol%, 1.5 vol%, and 0.5 vol% of meteorite, respectively.

Mineralogy and Mineral Chemistry

Olivine is the most abundant mineral in Jezersko. About 10% of all olivine grains show undulatory extinction and approximately 20% show planar fractures, while mosaicism was not observed. In the matrix, olivine is mostly subhedral to anhedral with poorly defined grain boundaries and is commonly associated with pyroxenes. Pyroxenes in the meteorite are represented by 68% low-Ca pyroxenes, while Ca-pyroxenes, mostly diopside, occupy 32% of the meteorite. Ca-pyroxenes were predominantly found in chondrules, particularly porphyritic and barred olivine-pyroxene, while in the matrix, they are scarce and were

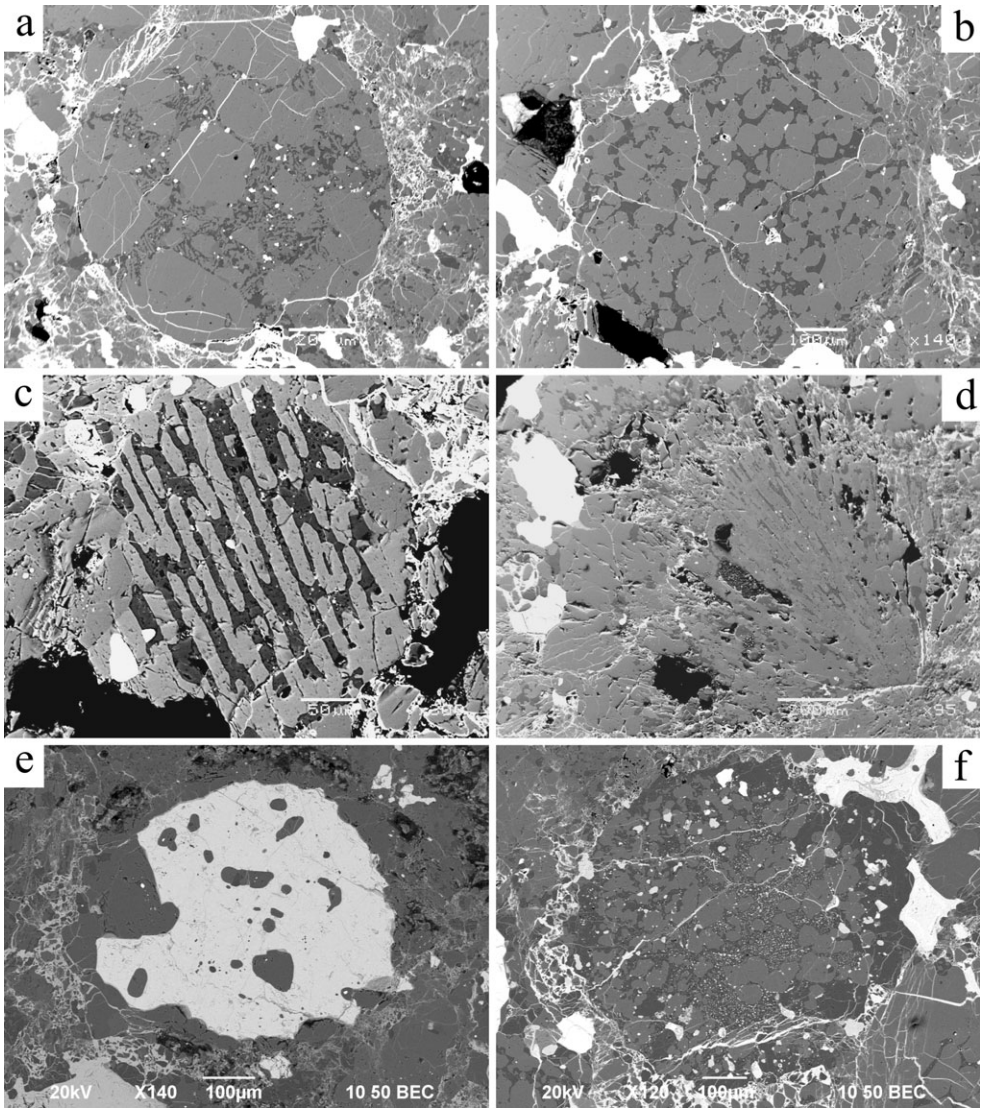

Fig. 2. SEM (BSE) images of typical chondrule textures in the Jezersko meteorite. a) Porphyritic olivine chondrule composed of idiomorphic olivine grains varying in size, xenomorphic pyroxene and matrix consisting of plagioclase and lath-shaped skeletal olivine crystals. b) Porphyritic olivine chondrule composed of tightly packed euhedral olivine grains. c) Barred olivine chondrule. d) Radial pyroxene chondrule. e) Metal chondrule composed of single troilite grain surrounded by coarse-grained olivine and pyroxene rim. f) Chromite-rich porphyritic olivine chondrule with chromite crystals in chondrule mesostasis.

only observed among metal-filled veins in the brecciated areas. XRD analysis showed that 34% of low-Ca pyroxenes belong to monoclinic variety clinoenstatite and 66% to orthorhombic enstatite. In composition, olivine is very homogeneous throughout the analyzed samples, in chondrules as well as in the matrix. The mean olivine composition, based on measurement of 142 olivine grains, is $Fa_{19.4 \pm 0.4}$ (Table 1). Low-Ca pyroxenes, found in chondrules, are compositionally less homogeneous compared with the ones found in the matrix. Their mean composition is $Fs_{16.7 \pm 0.3}$ ($n = 55$) (Table 1). Mean composition of 30 analyzed Ca-pyroxenes is $Fs_{6 \pm 1.2}$, $Wo_{45.8 \pm 1.4}$ (Table 1). The calculated mean FeO/MnO ratios in olivine, low-Ca pyroxene, and Ca-pyroxene are 36.9, 20.7, and 12.6, varying from 27.1 to 58, 16.2 to 27.2, and 7.9 to 29, respectively, which all lie within compositional ranges typical of H chondrites (Bunch and Wittke 2012). Anhedral plagioclase mostly forms chondrule mesostasis and also fills interstitial voids between matrix olivine and pyroxene; however, it is relatively scarce. The 44 analyzed plagioclases have mean composition of $Ab_{83 \pm 1.3}$, $An_{11 \pm 1.3}$, $Or_{6 \pm 1.3}$ (Table 1). Several large plagioclase grains with indicated cleavage and grain size of up to 193 μm containing small chromite crystals were found, which were interpreted as chromite-plagioclase

Table 1. Mean compositions and standard deviations (in wt%) of major minerals in Jezersko meteorite obtained by SEM/EDS analysis.

	Ol	Px	Px (Ca)	Plag	Apat	Mer	Chr	Kam	Tae	Ttae	Tro
n	142	55	30	44	11	27	41	51	35	8	45
O	41.5 ± 0.4	44.9 ± 0.3	43.1 ± 0.6	51.8 ± 0.8	40.6 ± 3.9	45.3 ± 1	35 ± 0.9	n.d.	n.d.	n.d.	n.d.
F	n.d.	n.d.	n.d.	n.d.	1.1 ± 0.6	n.d.	n.d.	n.d.	n.d.	n.d.	n.d.
Na	n.d.	n.d.	3 ± 2.4	6.5 ± 0.2	n.d.	1.8 ± 0.1	n.d.	n.d.	n.d.	n.d.	n.d.
Mg	25.6 ± 0.5	18.9 ± 0.3	10.1 ± 0.6	n.d.	n.d.	2.1 ± 0.2	1.8 ± 0.3	n.d.	n.d.	n.d.	n.d.
Al	n.d.	n.d.	0.4 ± 0.4	10.1 ± 0.2	n.d.	n.d.	3.1 ± 0.2	n.d.	n.d.	n.d.	n.d.
Si	18.4 ± 0.3	26.4 ± 0.2	24.5 ± 0.9	28.8 ± 0.6	n.d.	n.d.	n.d.	n.d.	n.d.	n.d.	n.d.
P	n.d.	n.d.	n.d.	n.d.	18.5 ± 1	20.7 ± 0.5	n.d.	n.d.	n.d.	n.d.	n.d.
S	n.d.	n.d.	n.d.	n.d.	n.d.	n.d.	n.d.	n.d.	n.d.	n.d.	38.6 ± 0.9
Cl	n.d.	n.d.	n.d.	n.d.	4.9 ± 0.3	n.d.	n.d.	n.d.	n.d.	n.d.	n.d.
K	n.d.	n.d.	n.d.	0.8 ± 0.2	n.d.	n.d.	n.d.	n.d.	n.d.	n.d.	n.d.
Ca	n.d.	0.5 ± 0.1	15.8 ± 1	1.5 ± 0.2	34.4 ± 2.7	30.2 ± 0.8	n.d.	n.d.	n.d.	n.d.	n.d.
Ti	n.d.	n.d.	0.2 ± 0.1	n.d.	n.d.	n.d.	1.2 ± 0.2	n.d.	n.d.	n.d.	n.d.
V	n.d.	n.d.	n.d.	n.d.	n.d.	n.d.	0.5 ± 0.1	n.d.	n.d.	n.d.	n.d.
Cr	n.d.	n.d.	0.5 ± 0.1	n.d.	n.d.	n.d.	36.7 ± 1.1	n.d.	n.d.	n.d.	n.d.
Mn	0.4 ± 0.1	0.4 ± 0.05	0.2 ± 0.05	n.d.	n.d.	n.d.	0.8 ± 0.2	n.d.	n.d.	n.d.	n.d.
Fe	14.1 ± 0.3	8.8 ± 0.2	2.9 ± 0.6	0.5 ± 0.4	0.9 ± 0.8	0.6 ± 0.2	20.8 ± 0.6	92.8 ± 2.5	69.2 ± 3.1	48.5 ± 2.5	61.1 ± 1.2
Ni	n.d.	n.d.	n.d.	n.d.	n.d.	n.d.	n.d.	6.6 ± 2.3	30.7 ± 3.4	50.1 ± 2.4	n.d.
FeO/MnO	36.9 ± 5.6	20.7 ± 2.6	12.6 ± 3.8	n.d.	n.d.	n.d.	n.d.	n.d.	n.d.	n.d.	n.d.
Cl/F	n.d.	n.d.	n.d.	n.d.	5.8 ± 3.4	n.d.	n.d.	n.d.	n.d.	n.d.	n.d.
Mg/(Mg+Fe)	n.d.	n.d.	n.d.	n.d.	n.d.	0.79 ± 0.07	n.d.	n.d.	n.d.	n.d.	n.d.
Fa	19.4 ± 0.4	n.d.	n.d.	n.d.	n.d.	n.d.	n.d.	n.d.	n.d.	n.d.	n.d.
Fs	n.d.	16.7 ± 0.3	6 ± 1.2	n.d.	n.d.	n.d.	n.d.	n.d.	n.d.	n.d.	n.d.
Wo	n.d.	1.2 ± 0.3	8 ± 1.4	n.d.	n.d.	n.d.	n.d.	n.d.	n.d.	n.d.	n.d.
Ab	n.d.	n.d.	n.d.	83 ± 1.3	n.d.	n.d.	n.d.	n.d.	n.d.	n.d.	n.d.
An	n.d.	n.d.	n.d.	11 ± 1.3	n.d.	n.d.	n.d.	n.d.	n.d.	n.d.	n.d.
Or	n.d.	n.d.	n.d.	6 ± 1.3	n.d.	n.d.	n.d.	n.d.	n.d.	n.d.	n.d.
Cr/(Cr+Al)[a]	n.d.	n.d.	n.d.	n.d.	n.d.	n.d.	0.86 ± 0.01	n.d.	n.d.	n.d.	n.d.
Fe/(Fe+Mg)[a]	n.d.	n.d.	n.d.	n.d.	n.d.	n.d.	0.83 ± 0.02	n.d.	n.d.	n.d.	n.d.

n = number of analyses; n.d. = not detected; Ol = olivine; Px = low-Ca pyroxene; Px (Ca) = Ca-pyroxene; Plag = plagioclase; Apat = apatite; Mer = merrillite; Chr = chromite; Kam = kamacite; Tae = taenite; Ttaen = tetrataenite; Tro = troilite.

[a]In mole%.

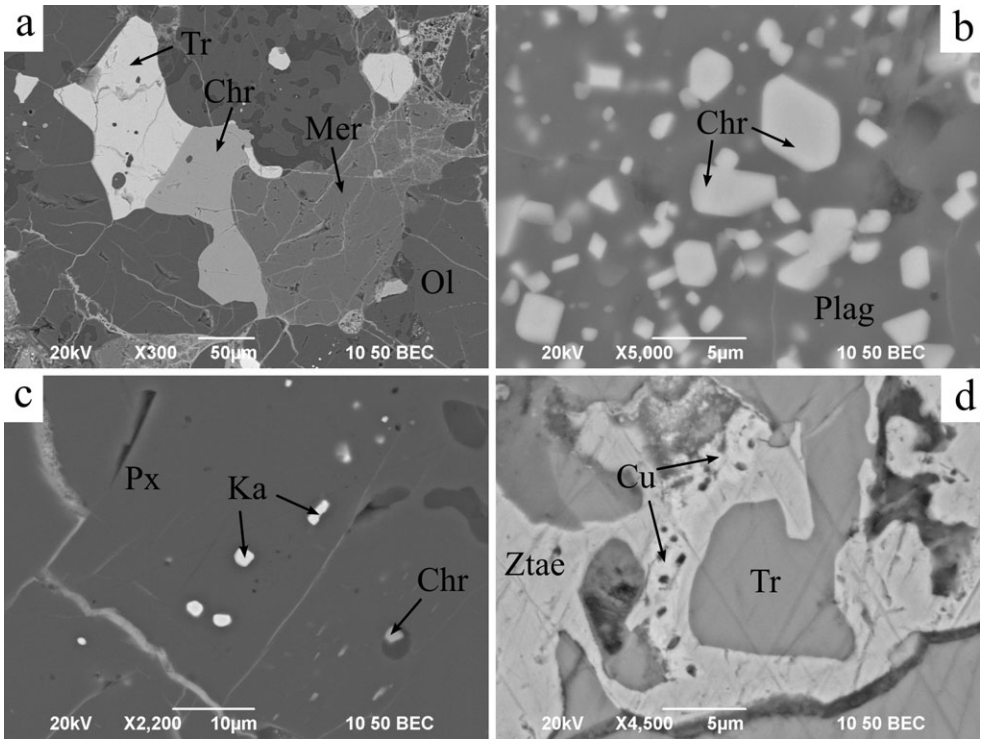

Fig. 3. SEM (BSE) images of phosphates and metallic minerals in Jezersko meteorite. a) Fractured field of merrillite (Me) associated with chromite (Chr) and troilite (Tr). b) Euhedral chromite crystals (Chr) in the plagioclase mesostasis (Plag) of chromite-rich chondrule. c) Micron-sized kamacite (Ka) and chromite (Chr) inclusions in meteorite matrix pyroxene (Px). d) Troilite grain (Tr) rimmed by zoned taenite (Ztae) with inclusions of metallic Cu.

assemblages. Plagioclases in some of these assemblages are zoned. Their composition ranges from the Ca-rich plagioclase (oligoclase or andesine) in the center to the Na-rich plagioclase (albite) on the outer edge.

Phosphates are represented by large heavily fractured irregular fields of Cl-apatite and strongly dominating merrillite (Fig. 3a) with mean sizes of 100 and 243 μm, respectively, associated with chromite and troilite. They are also present in chondrule mesostasis and as rounded inclusions in chromite. The mean Cl/F ratio in Cl-apatite in Jezersko is 5.8 (Table 1) and corresponds to the ratio in some H5 chondrites (Jones and McCubbin 2012). The mean Mg/(Mg+Fe) ratio in Jezersko merrillite is 0.79 (Table 1), ranging between 0.65 and 0.94, which is below the ratio in H chondrites (Kleinschrot 1997), but the wide range is consistent with ranges in L chondrites of petrologic type 4 (Lewis and Jones 2013).

Chromite occurs in the meteorite matrix and in chondrules. In the matrix, it forms small rounded inclusions in pyroxene and large subhedral to euhedral grains with mean size of 120 μm, associated with zoned taenite, troilite, and merrillite. In chromite-rich POP and BOP chondrules, chromite occurs in the plagioclase mesostasis (Fig. 3b), also in some olivine and pyroxene crystals, as randomly oriented euhedral grains with mean grain size of 49 μm or forms arrays of acicular euhedral crystals oriented in one direction. Chromite in mesostasis of chromite-rich chondrules indicates they are of secondary origin, formed during melting of chromite and silicates after a high-energy shock event, followed by rapid crystallization (Rubin 2003). The calculated mean Cr/(Cr+Al) and Fe/(Fe+Mg) ratios in chromites are relatively low and amount to 0.86 and 0.83 (Table 1), respectively, which is in agreement with H chondrites of petrologic type 4, according to Wlotzka (2005). Several large chromite-plagioclase assemblages were found in the meteorite matrix. Micron-sized chromite inclusions within these assemblages are concentrated mostly in and around the center of plagioclase and have higher Al content than chromites in the matrix. According to Rubin (2003), these assemblages also indicate high-temperature shock metamorphosis.

Kamacite occurs as variable sized anhedral fields in the meteorite matrix with mean size of 304 μm containing spherical silicate inclusions. It also forms micron-sized subhedral to euhedral inclusions in matrix olivine and pyroxene (Fig. 3c). In chondrules, low-Ni kamacite occurs as parallel lath-like inclusions in pyroxenes. Taenite is zoned and exhibits M-shaped Ni profiles that formed at 500–600 °C (Wood 1964; Willis

and Goldstein 1981). Larger taenite grains frequently have martensitic interiors. In the meteorite matrix, taenite occurs as large irregularly shaped fields with mean size of 123 μm that contain troilite and silicate inclusions, while in chondrules, taenite is spherically shaped. Unzoned tetrataenite, which formed during slow cooling below 350 °C (Clarke and Scott 1980), is associated with taenite and kamacite and envelopes other minerals, particularly troilite. Independent tetrataenite grains in the meteorite matrix are irregularly shaped and are up to 64 μm in size. Tetrataenite composition is relatively homogeneous (Table 1). Plessite is present in meteorite matrix as well as in chondrules and forms large irregular fields within zoned taenite or is associated with troilite.

Troilite is homogeneously distributed throughout the sample. In the matrix, it occurs as irregular fields or fractured grains with a mean size of 195 μm forming straight grain boundaries with the matrix silicates. Fractures are commonly filled with oxidized Fe-Ni metal. Some troilite grains contain spherical micron-sized inclusions of forsterite, enstatite, and molybdenum sulfide and also Ni-bearing sulfide grains between adjacent troilite grains. Troilite is commonly associated with taenite and kamacite forming rounded anhedral inclusions rimmed by zoned taenite with transition to unzoned tetrataenite (Fig. 3d), which is consistent with unshocked to moderately shocked chondrites (Scott et al. 2010). According to Scott et al. (2010), zoned taenite and unzoned tetrataenite formed after formation of troilite as a result of diffusion of Ni from troilite. Larger anhedral troilite grains are commonly rimming chondrules. In chondrules, troilite grains of mean size of 45 μm occur as large individual grains in plagioclase mesostasis and as euhedral grains connecting adjacent olivine crystals. Elongated troilite inclusions in olivine crystals, oriented parallel to the longer axis of olivine, were also found.

Along some taenite–troilite boundaries, scarce elongated anhedral exsolutions of metallic Cu with dimensions of 16 × 2.5 μm and 10.5 × 8 μm were found in zoned taenite (Fig. 3d). This type of occurrence of metallic Cu presumably formed with localized melting of troilite–Fe–Ni metal associations during high-temperature shock metamorphosis followed by exsolution of metallic Cu from taenite (Rubin 2004; Tomkins 2009).

Molybdenum sulfide was found as a 7 × 2 μm large subhedral lath-like inclusion completely enclosed in a large irregularly shaped field of pure troilite associated with two BO chondrules (Figs. 4a and 4b). It contains 3.2 wt% O, 31.6 wt% S, 21 wt% Fe, and 44.2 wt% Mo. According to atomic ratio between Mo and S it is most probably molybdenite. Molybdenite inclusions, reported in high-Ni metal in carbonaceous chondrites, probably formed through conversion of metastable Mo_2S_3, which originated in the solar nebula and represents the nucleation site for condensation of metastable troilite (Fuchs and Blander 1977). At lower temperature, the Mo_2S_3 was converted to molybdenite through reaction with troilite (Fuchs and Blander 1977). As molybdenite in the Jezersko meteorite occurs within troilite, it could have formed in similar way.

Ni-bearing sulfide, containing 35.7 wt% S, 45.1 wt% Fe, and 18.3 wt% Ni, occurs as a 7 × 9 μm large euhedral hexagonal-like inclusion in troilite between adjacent troilite grains (Fig. 4c). Atomic ratios between Fe, Ni, and S showed that this Ni-bearing sulfide is most probably pentlandite or a phase intermediate between pyrrhotite and pentlandite, a monosulfide solid solution according to Zolensky and Le (2003). According to Lauretta et al. (1997a), pentlandite in carbonaceous chondrites formed by sulfurization of Fe-Ni metal in the solar nebula by fast diffusion of Ni from metal through adjacent sulfide to its outer edge at the interface with S-bearing gas, where pentlandite inclusions formed. In ordinary chondrites, compositions of pentlandite and host sulfide grains were mostly equilibrated due to thermal metamorphism (Lauretta et al. 1997b).

In corrosion pits around some troilite grains, at the interface between troilite and olivine, about 5 × 2 μm large corroded inclusions of partly oxidized Ni- and Co-rich sulfide phases occur (Fig. 4d), which are most probably cobaltpentlandite as indicated by their compositions (21.5 wt% O, 19.1 wt% S, 13.4 wt% Fe, 39.2 wt% Ni, 6.2 wt% Co, and 1.3 wt% Cu).

Shock Metamorphism and Weathering

As stated above, about 10% of olivine grains show undulatory extinction and approximately 20% of olivine grains contain distinct planar fractures, indicating that Jezersko meteorite is a very weakly shocked meteorite of shock stage S2, according to shock-stage scale by Stöffler et al. (1991). However, most chondrules are severely fractured and fragmented. Matrix that surrounds chondrules is commonly brecciated and cut by shock veins and pockets filled with oxidized metal. Also other petrographic shock indicators, such as chromite-plagioclase assemblages, irregularly shaped troilite inclusions in Fe-Ni metal, Fe-Ni metal veins, metallic Cu, and normal Ni profiles measured in most of taenite grains, are consistent with shock stage S3, according to shock metamorphic features defined by Bennett and McSween (1996) and Rubin (2004).

The residence time of meteorite Jezersko on the ground and time of its exposure to weathering, before

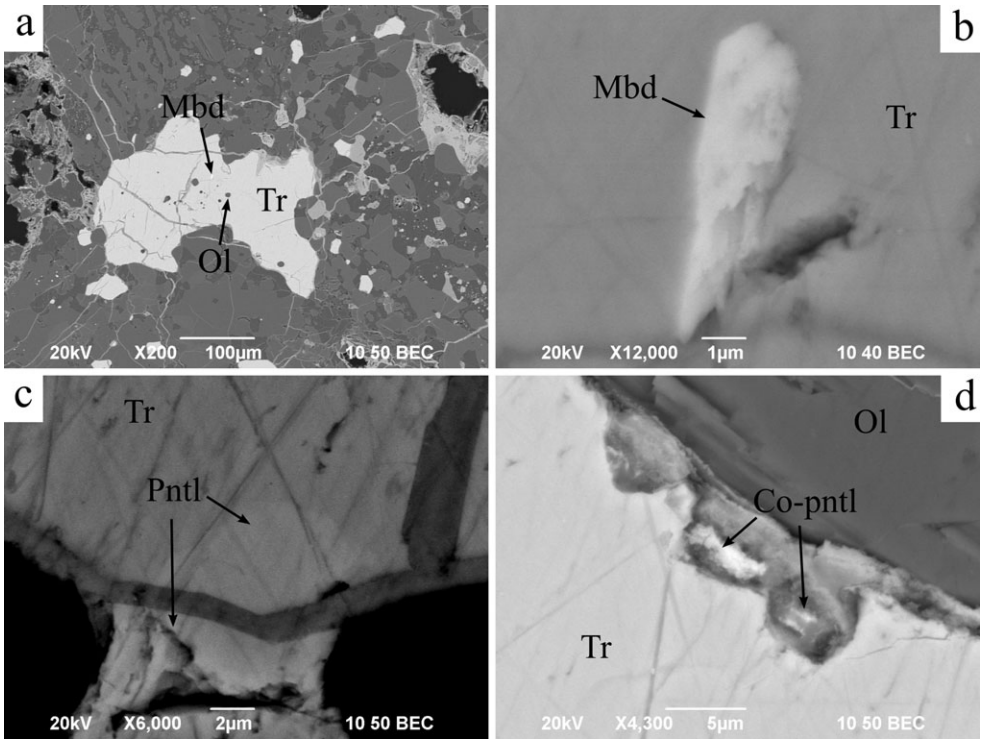

Fig. 4. SEM (BSE) images of rare sulfide minerals in Jezersko meteorite. a) Molybdenite (Mbd) inclusion enclosed in troilite (Tr) containing rounded olivine (Ol) inclusions. b) Detail of lath-like molybdenite (Mbd) in troilite (Tr). c) Pentlandite (Pntl) inclusion in troilite (Tr) between adjacent troilite grains. d) Cobaltpentlandite (Co-pntl) inclusion in corrosion pit in troilite (Tr) at the troilite (Tr)–olivine (Ol) interface.

its recovery in 1992, are not yet known. However, weathering processes partially altered the meteorite. Some parts of the fusion crust turned from brownish to orange yellow color due to oxidation. Veins of secondary iron oxides and hydroxides are also present in the meteorite interior, replacing up to 30% of metal. All these signs indicate that meteorite Jezersko is a moderately weathered meteorite with a weathering grade of W2, according to the classification for ordinary chondrites proposed by Wlotzka (1993). Based on its moderate weathering grade it can be assumed that the meteorite was recovered within a year after the fall; however, the exact terrestrial age has not been determined yet.

Chemical Composition

The bulk chemical composition of major and trace elements in meteorite Jezersko is given in Table 2 together with average compositions of H and L chondrites (Lodders and Fegley 1998). Element abundances normalized to Mg and CI chondrites (Anders and Grevesse 1989) are shown in Fig. 5. Abundances of lithophile elements mostly correspond to the mean H chondrite composition, with the exception of most lanthanides, whose contents are closer to L chondrites. According to Mg and CI normalized abundances (Fig. 5), most of the lithophiles in Jezersko meteorite fall between H and L chondrites, while abundances of most of lanthanides, Ba, K, and Rb are much higher than those of H and L chondrites. Siderophile elements, especially platinum group, generally differ in contents from H chondrites, while abundances of chalcophiles in Jezersko are quite close to those in H chondrites, with the exception of Se and S.

Abundances of refractory siderophile elements Re, Ru, Rh, and Os are much below those in H and L chondrites, while more volatile siderophiles fall between H and L chondrites. High abundance of Mo in Jezersko is consistent with the presence of molybdenite. As Re and Ru have already been reported to be more susceptible to oxidation and more mobile elements (Palme et al. 1998; Horan et al. 2003), this could be interpreted as a consequence of the more oxidized character of the Jezersko meteorite parent body. The calculated ratios between refractory lithophile elements and Si, such as Mg/Si (8.12×10^{-1}), are in agreement with ratios in H chondrites and also with values in some other reported H chondrites (e.g., Dhingra et al. 2004; Reimold et al. 2004). Calculated ratios between siderophile and lithophile elements Fe/Mg, Fe/Si, Ir/Mg,

Table 2. Bulk chemical composition of the Jezersko meteorite compared with average compositions of H and L chondrites (Lodders and Fegley 1998).

Element	Unit	Method	Jezersko	H chondrites	L chondrites
Na	μg g^{-1}	FUS-ICP/OES	5900	6110	6900
Mg	wt%	FUS-ICP/OES	13.82	14.1	14.9
Al	wt%	FUS-ICP/OES	1.09	1.06	1.16
Si	wt%	FUS-ICP/OES	17.02	17.1	18.6
P	μg g^{-1}	FUS-ICP/OES	1047	1200	1030
S	wt%	TD-ICP/OES	1.49	2	2.2
K	μg g^{-1}	FUS-ICP/OES	996	780	920
Ca	wt%	FUS-ICP/OES	1.19	1.22	1.33
Sc	μg g^{-1}	INAA	7.6	7.8	8.1
Ti	μg g^{-1}	FUS-ICP/OES	594	630	670
V	μg g^{-1}	FUS-ICP/OES	68	73	75
Cr	μg g^{-1}	FUS-ICP/MS	3310	3500	3690
Mn	μg g^{-1}	FUS-ICP/OES	2370	2340	2590
Fe	wt%	INAA	25.1	27.2	21.75
Co	μg g^{-1}	INAA	727	830	580
Ni	wt%	FUS-ICP/OES	1.5	1.71	1.24
Cu	μg g^{-1}	FUS-ICP/MS	90	94	90
Zn	μg g^{-1}	FUS-ICP/MS	50	47	57
Ga	μg g^{-1}	FUS-ICP/MS	6	6	5.4
Ge	μg g^{-1}	FUS-ICP/MS	13	10	10
As	μg g^{-1}	INAA	<0.5	2.2	1.36
Se	μg g^{-1}	INAA	12	8	8.5
Br	μg g^{-1}	INAA	<0.5	<1	<2
Rb	μg g^{-1}	FUS-ICP/MS	3	2.3	2.8
Sr	μg g^{-1}	FUS-ICP/OES	11	8.8	11
Mo	μg g^{-1}	FUS-ICP/MS	2	1.4	1.2
Ru	μg kg^{-1}	Ni-FINA	535	1100	750
Rh	μg kg^{-1}	Ni-FINA	123	210	155
Pd	μg kg^{-1}	Ni-FINA	565	845	620
Sb	μg kg^{-1}	INAA	<100	66	78
Cs	μg kg^{-1}	FUS-ICP/MS	<500	<200	<500
Ba	μg g^{-1}	FUS-ICP/OES	5	4.4	4.1
La	μg kg^{-1}	FUS-ICP/MS	600	301	318
Ce	μg kg^{-1}	FUS-ICP/MS	1100	763	970
Pr	μg kg^{-1}	FUS-ICP/MS	150	120	140
Nd	μg kg^{-1}	FUS-ICP/MS	700	581	700
Sm	μg kg^{-1}	INAA	200	194	203
Eu	μg kg^{-1}	FUS-ICP/MS	60	74	80
Gd	μg kg^{-1}	FUS-ICP/MS	300	275	317
Dy	μg kg^{-1}	FUS-ICP/MS	300	305	372
Er	μg kg^{-1}	FUS-ICP/MS	200	213	252
Yb	μg kg^{-1}	FUS-ICP/MS	200	203	226
Re	μg kg^{-1}	Ni-FINA	28	78	47
Os	μg kg^{-1}	Ni-FINA	356	835	530
Ir	μg kg^{-1}	INAA	699	770	490
Pt	μg g^{-1}	Ni-FINA	1.1	1.58	1.09
Au	μg kg^{-1}	Ni-FINA	149	220	156

FUS-ICP/MS = fusion inductively coupled plasma mass spectrometry; FUS-ICP/OES = fusion inductively coupled plasma optical emission spectrometry; INAA = instrumental neutron activation analysis; Ni-FINA = nickel sulfide fire assay instrumental neutron activation analysis; TD-ICP/OES = total digestion inductively coupled plasma optical emission spectrometry.

and Ir/Si are 1.82, 1.47, 5.06×10^{-6}, and 4.11×10^{-6}, respectively. They are somewhat lower than ratios calculated from the mean H chondrite composition. Lower siderophile versus lithophile ratios in Jezersko could indicate that it is a more oxidized H chondrite, while lower siderophile versus Si ratios, especially Ir/Si,

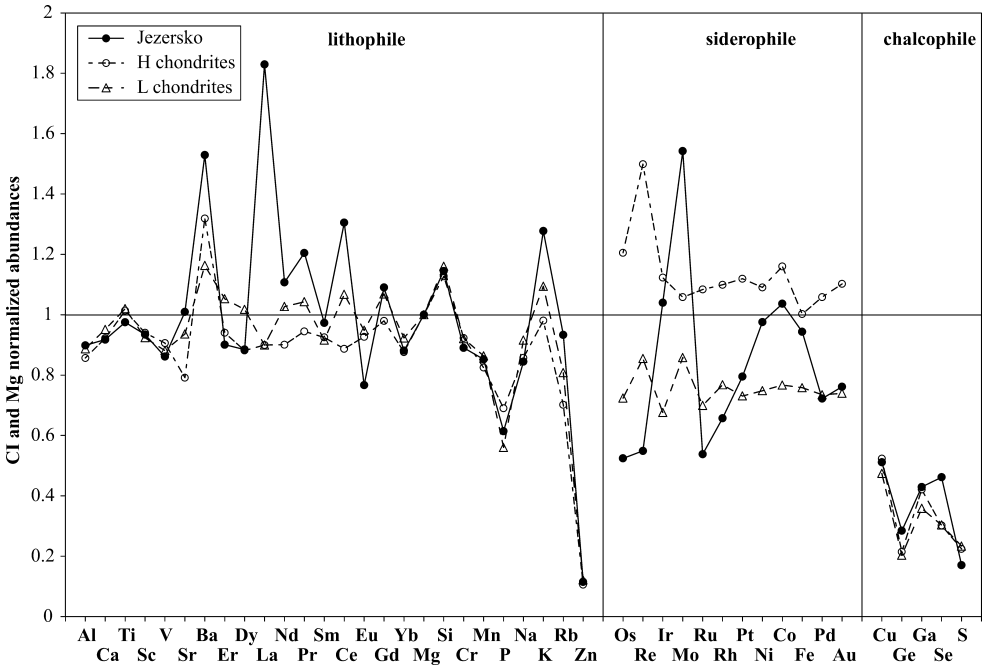

Fig. 5. Abundances of lithophile, siderophile, and chalcophile elements in Jezersko meteorite, H and L chondrites normalized to Mg and CI chondrites and arranged from left to right in order of increasing volatility. The CI chondrite values are from Anders and Grevesse (1989) and H and L chondrite values from Lodders and Fegley (1998).

could be explained by incomplete metal-silicate fractionation accompanied by increasing oxidation, which is in agreement with findings of Rubin et al. (1986) and Mittlefehldt et al. (2008). Oxidized character of the Jezersko meteorite parent body is also supported by generally very low refractory versus volatile siderophile element ratios, such as Ir/Ga (1.17×10^{-1}) and Pt/Ga (1.83×10^{-1}), as compared with H chondrites.

Some variations in element contents in Jezersko meteorite could be partly ascribed to terrestrial weathering, which also affected the interior of the meteorite. However, according to Wolf and Lipschutz (1995), contents of labile trace elements are not significantly altered by weathering; thus, most deviations in contents of these elements in Jezersko from the mean H chondrite composition were assumed to occur as a consequence of inhomogeneous composition of the parent body.

Classification of Meteorite Jezersko

Most of the measured features of Jezersko agree well with H group chondrites. Based on composition of olivine and low-Ca pyroxene, Jezersko meteorite belongs to the H group of ordinary chondrites, which is also supported by relatively low calculated mean FeO/MnO ratios in olivine, low-Ca pyroxene, and Ca-pyroxene (Bunch and Wittke 2012). Modal abundance of metallic minerals is high and corresponds to H chondrites. Contents of lithophile elements in Jezersko and ratios between refractory lithophile elements and Si mostly agree with composition of H chondrites. The texture of meteorite Jezersko is partially recrystallized, but chondrules are still clearly discernible. Very homogeneous compositions of olivine and pyroxene in chondrules and in the meteorite matrix indicate that meteorite Jezersko is of petrologic type 4, which is also supported by the quantity of monoclinic low-Ca pyroxenes (34%) (Weisberg et al. 2006). The mean Cr/(Cr+Al) and Fe/(Fe+Mg) ratios in chromite are also in agreement with H4 chondrites (Wlotzka 2005). Scarce olivine grains with undulatory extinction and planar fractures are in agreement with lower shock stages (S2). However, the presence of heavily fractured chondrules, brecciated matrix, large pockets of Fe-Ni metal, chromite-plagioclase assemblages, chromite-rich chondrules, metallic Cu, and M-shaped Ni profiles measured across taenite grains are consistent with shock stage S3 (Bennett and McSween 1996; Rubin 2004). Low contents of siderophile elements and their ratios with lithophile elements indicate that meteorite Jezersko is a more oxidized H chondrite (Rubin et al. 1986). By considering the most important classification factors, meteorite Jezersko was thus classified as an H4 S2(3) ordinary chondrite.

Some of the measured physical and chemical properties of Jezersko meteorite seem to be indicative of L group chondrites. Very large mean chondrule diameter is not consistent with H chondrites and falls in

the range typical of L chondrites. The wide range of Mg/(Mg+Fe) ratios in merrillite is consistent with ranges in L chondrites of petrologic type 4 (Lewis and Jones 2013). Very high bulk contents of lanthanides in Jezersko are closer to L chondrites as well.

Thermal History of Meteorite Jezersko

The interpretation of the Jezersko meteorite thermal history was based on various geothermometers and metallographic cooling rates. A peak metamorphic temperature of 854 °C ± 41 °C, ranging from 784 to 922 °C, was calculated for the Jezersko meteorite using the orthopyroxene/clinopyroxene thermometer of Ganguly et al. (2013). This calculated temperature is very high and is closer to H5 than H4 chondrites, according to temperatures proposed by Monnereau et al. (2013). The mean equilibration temperature of Jezersko chondrite, which was calculated using olivine-chromite thermometer based on an equation by Wlotzka (2005), is 687 °C ± 27 °C, ranging between 641 and 740 °C (Fig. 6a), and is very close to olivine-chromite temperatures of H4 (e.g., Foster, Daraj 012) and H5 (e.g., Flandreau, Daraj 020, Richardton) chondrites reported in Wlotzka (2005). According to Wlotzka (2005), temperatures obtained from chromite are 50–100 °C lower than those obtained from Cr-spinel. Thus, the corrected mean temperature is between 737 and 787 °C. These temperatures are still much lower than that inferred from two-pyroxene thermometer, possibly due to difference in closure temperatures of pyroxenes and olivine-chromite or poor clinopyroxene equilibration (Wlotzka 2005). The approximate final equilibration temperature of the Jezersko meteorite, estimated from compositions of coexisting olivine and orthopyroxene plotted in a diagram of olivine-orthopyroxene composition between 900 and 500 °C constructed by Reisener et al. (2006), is about 750 °C, which roughly corresponds to the corrected equilibration temperature obtained from olivine-chromite pairs. The cooling rate of meteorite Jezersko in the temperature range between 450 and 600 °C was estimated from metallographic data based on the correlation between the central Ni content and the half-width of taenite (Willis and Goldstein 1981). The obtained cooling rate is 10 °C Myr^{-1} (Fig. 6b), which is at the lower end of the range typical of equilibrated H chondrites (Scott et al. 2013, 2014) and is similar to weakly shocked H4 meteorites (e.g., Ankober, Marilia, Ochansk) (Scott et al. 2014). Homogeneous composition of olivine and pyroxenes and high peak metamorphic temperatures indicate that Jezersko was located relatively deep within the primary parent body and experienced thermal metamorphism, which equilibrated composition of silicates. Lack of compositional zoning in pyroxenes, i.e., Mg concentration profiles across orthopyroxenes are flat and steeply decrease toward clinopyroxenes, reflects relatively fast cooling at temperatures above 700 °C after equilibration, which is in agreement with findings of Ganguly et al. (2013), indicating that the parent body was probably disrupted by impact soon after the peak metamorphic temperatures were attained, leading to fast cooling. The low metallographic cooling rate in Jezersko indicates that the parent body must have reaccreted soon after disruption before the material cooled down below 600 °C, in order for taenite to develop Ni concentration gradients as suggested by Scott et al. (2014), and that Jezersko

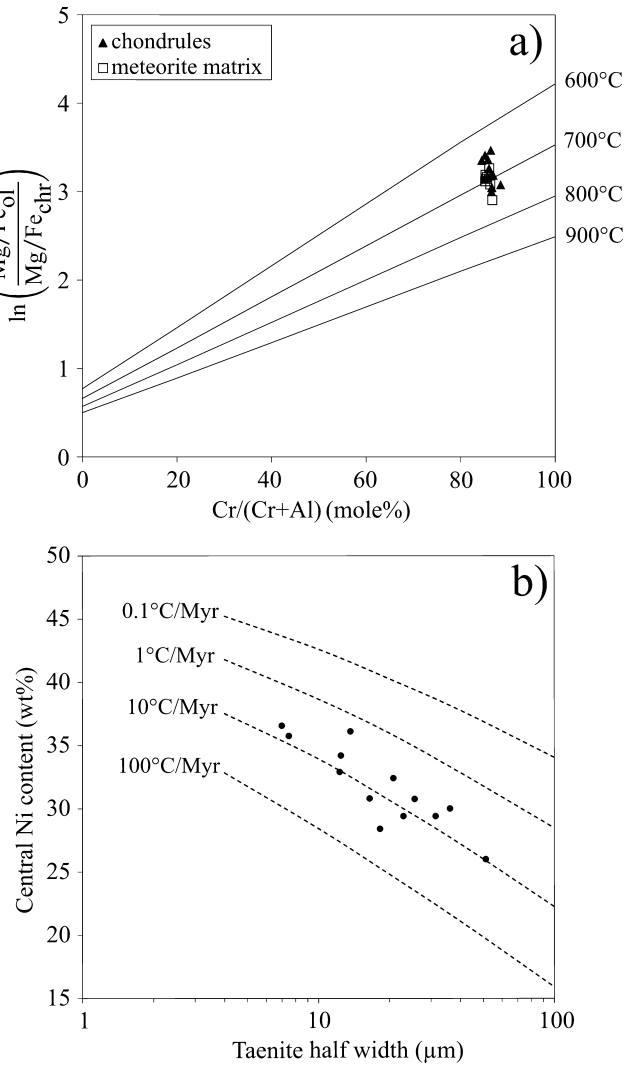

Fig. 6. Thermal history of meteorite Jezersko. a) Olivine (ol)-chromite (chr) isotherm diagram for chromites in chondrules and meteorite matrix based on Wlotzka (2005). b) Central Ni content versus taenite half-width plotted on a diagram of metallographic cooling rate curves based on Willis and Goldstein (1981).

meteorite material was buried deeper in the reaccreted parent body.

Acknowledgments—The authors acknowledge the financial support from the state budget of the Slovenian Research Agency obtained through the research programs "Groundwater and geochemistry" (No. P1-0020), and "Mineral resources" (No. P1-0025). We are grateful to technical co-workers Miran Udovč and Mladen Štumergar for help with the preparation of samples. We also thank Dr. Edward R. D. Scott and Dr. Jon M. Friedrich for their critical reviews and helpful comments.

Editorial Handling—Dr. Edward Scott

REFERENCES

Activation Laboratories. 2013. *2013 International Schedule of Services and Fees*. Ancaster, Ontario, Canada: Activation Laboratories Ltd. 34 p.

Anders E. and Grevesse N. 1989. Abundances of the elements: Meteoritic and solar. *Geochimica et Cosmochimica Acta* 53:197–214.

Bennett M. E. III and McSween H. Y. Jr. 1996. Shock features in iron-nickel metal and troilite of L-group ordinary chondrites. *Meteoritics & Planetary Science* 31:255–264.

Bunch T. E. and Wittke J. H. 2012. *Classification handbook: Ordinary chondrites*. http://www4.nau.edu/meteorite/Meteorite/OrdChondrites.html.

Clarke R. S. and Scott E. R. D. 1980. Tetrataenite-ordered Fe-Ni, a new mineral in meteorites. *American Mineralogist* 65:624–630.

Dhingra D., Bhandari N., Shukla P. N., Murty S. V. S., Mahajan R. R., Ballabh G. M., Lashkari G., Shukla A. D., and Parthasarathy G. 2004. Spectacular fall of the Kendrapara H5 chondrite. *Meteoritics & Planetary Science* 39:A121–A132.

Donaldson C. H. 1976. An experimental investigation of olivine morphology. *Contributions to Mineralogy and Petrology* 57:187–195.

Fuchs L. H. and Blander M. 1977. Molybdenite in calcium-aluminum-rich inclusions in the Allende meteorite. *Geochimica et Cosmochimica Acta* 41:1170–1175.

Ganguly J., Tirone M., Chakraborty S., and Domanik K. 2013. H-chondrite parent asteroid: A multistage cooling, fragmentation and re-accretion history constrained by thermometric studies, diffusion kinetic modeling and geochronological data. *Geochimica et Cosmochimica Acta* 105:206–220.

Greshake A., Wolfgang K., Arndt P., Maetz M., Flynn G. J., and Bischoff A. 1998. Heating experiments simulating atmospheric entry heating of micrometeorites: Clues to parent body sources. *Meteoritics & Planetary Science* 33:267–290.

Horan M. F., Walker R. J., Morgan J. W., Grossman J. N., and Rubin A. E. 2003. Highly siderophile elements in chondrites. *Chemical Geology* 196:5–20.

Jones R. H. and McCubbin F. M. 2012. Phosphate mineralogy and the bulk chlorine/fluorine ratio of ordinary chondrites (abstract #2029). 43rd Lunar and Planetary Science Conference. CD-ROM.

Kleinschrot D. 1997. *Die Chondrite und ausgewählte Eisenmeteorite aus der Meteoritensammlung der Universität Würzburg*. Marburg: Tectum-Verlag. 188 p.

Lauretta D. S., Lodders K., Fegley B. Jr., and Kremser D. T. 1997a. The origin of Ni-bearing sulfides in CI carbonaceous chondrites. Proceedings, 28th Lunar and Planetary Science Conference. pp. 783–784.

Lauretta D. S., Lodders K., and Fegley B. Jr. 1997b. The alteration of Ni-bearing sulfides during thermal metamorphism on ordinary chondrite parent bodies. In *Workshop on parent body and nebula modification of chondritic materials*, edited by Zolensky M. E., Krot A. N. and Scott E. R. D. LPI Contribution 97-02, Part 1. Houston, Texas: Lunar and Planetary Institute. pp. 36–38.

Lewis J. A. and Jones R. H. 2013. Phosphate mineralogy of petrologic type 4-6 L ordinary chondrites (abstract #2722). 44th Lunar and Planetary Science Conference. CD-ROM.

Lodders K. and Fegley B. Jr. 1998. *The planetary scientist's companion*. New York: Oxford University Press. 371 p.

Mioč P. 1983. *Basic geological map of SFRJ 1:100.000, explanatory text of sheet Ravne na Koroškem*. Belgrade: Federal Geological Survey. 69 p.

Mittlefehldt D. W., Clayton R. N., Drake M. J., and Righter K. 2008. Oxygen isotopic composition and chemical correlations in meteorites and the terrestrial planets. In *Oxygen in the solar system*, edited by MacPherson G. J., Mittlefehldt D. W., and Jones J. H. Reviews in Mineralogy and Geochemistry, vol. 68. Chantilly, Virginia: Mineralogical Society of America. pp. 399–428.

Monnereau M., Toplis M. J., Baratoux D., and Guignard J. 2013. Thermal history of the H-chondrite parent body: Implications for metamorphic grade and accretionary time-scales. *Geochimica et Cosmochimica Acta* 119:302–321.

Oxford Instruments. 2006. *INCA energy operator manual*. High Wycombe, UK: Oxford Instruments Analytical Ltd. p. 85.

Palme H., Borisov A., and Wulf A. V. 1998. Experimental determination of the oxidation sequence of refractory metals (abstract #1611). 29th Lunar and Planetary Science Conference. CD-ROM.

Reimold W. U., Buchanan P. C., Ambrose D., Koeberl C., Franchi I., Lalkhan C., Schultz L., Franke L., and Heusser G. 2004. Thuathe, a new H4/5 chondrite from Lesotho: History of the fall, petrography, and geochemistry. *Meteoritics & Planetary Science* 39:1321–1341.

Reisener R. J., Goldstein J. I., and Petaev M. I. 2006. Olivine zoning and retrograde olivine-orthopyroxene-metal equilibration in H5 and H6 chondrites. *Meteoritics & Planetary Science* 41:1839–1852.

Rubin A. E. 2003. Chromite-Plagioclase assemblages as a new shock indicator; implications for the shock and thermal histories of ordinary chondrites. *Geochimica et Cosmochimica Acta* 67:2695–2709.

Rubin A. E. 2004. Postshock annealing and postannealing shock in equilibrated ordinary chondrites: Implications for the thermal and shock histories of chondritic asteroids. *Geochimica et Cosmochimica Acta* 68:673–689.

Rubin A. E., Kallemeyn G. W., and Wasson J. T. 1986. The continuous nebular fractionation sequence within H-group

chondrites. Proceedings, 17th Lunar and Planetary Science Conference. pp. 734–735.
Scott E. R. D. and Krot A. N. 2003. Chondrites and their components. In *Treatise on Geochemistry*, vol. 1, edited by Holland H. D. and Turekian K. K. Amsterdam: Elsevier. pp. 143–200.
Scott E. R. D., Goldstein J. I., and Yang J. 2010. Early impact history of ordinary chondrite parent bodies inferred from troilite-metal intergrowths (abstract #5031). *Meteoritics & Planetary Science* 45:A184.
Scott E. R. D., Krot T. V., and Goldstein J. I. 2013. Thermal and impact histories of ordinary chondrites and their parent bodies: Constraints from metallic Fe-Ni in type 3 chondrites (abstract #1826). 44th Lunar and Planetary Science Conference. CD-ROM.
Scott E. R. D., Krot T. V., Goldstein J. I., and Wakita S. 2014. Thermal and impact history of the H chondrite parent asteroid during metamorphism: Constraints from metallic Fe–Ni. *Geochimica et Cosmochimica Acta* 136:13–37.
Sears D. 2004. *The origin of chondrules and chondrites*. Cambridge: Cambridge University Press. 209 p.
Sokol A. and Bischoff A. 2005. Meteorites from Botswana. *Meteoritics & Planetary Science* 40:A177–A184.
Stöffler D., Keil K., and Scott E. R. D. 1991. Shock metamorphism of ordinary chondrites. *Geochimica et Cosmochimica Acta* 55:3845–3867.
Tomkins A. G. 2009. What metal-troilite textures can tell us about post-impact metamorphism in chondrite meteorites. *Meteoritics & Planetary Science* 44:1133–1149.
Weisberg M. K., McCoy T. J., and Krot A. N. 2006. Systematics and evaluation of meteorite classification. In *Meteorites and the early solar system II*, edited by Lauretta D. S., and McSween H. Y. Jr. Tucson, Arizona: The University of Arizona Press. pp. 19–52.
Willis J. and Goldstein J. I. 1981. A revision of metallographic cooling rate curves for chondrites. Proceedings, 12th Lunar and Planetary Science Conference. pp. 1135–1143.
Wlotzka F. A. 1993. Weathering scale for the ordinary chondrites. *Meteoritics* 28:460–460.
Wlotzka F. A. 2005. Cr spinel and chromite as petrogenetic indicators in ordinary chondrites: Equilibration temperatures of petrologic types 3.7 to 6. *Meteoritics & Planetary Science* 40:1673–1702.
Wolf S. F. and Lipschutz M. E. 1995. Chemical studies of H chondrites—7. Contents of Fe^{3+} and labile trace elements in Antarctic samples. *Meteoritics* 30:621–623.
Wood J. A. 1964. The cooling rates and parent planets of several iron meteorites. *Icarus* 3:429–459.
Zolensky M. E. and Le L. 2003. Iron-nickel sulfide compositional ranges in CM chondrites: No simple plan (abstract #1235). 34th Lunar and Planetary Science Conference. CD-ROM.